The Accurate Assessment of Muscle Excitation Requires the Detection of Multiple Surface Electromyograms

Bis-ferrocene molecular QCA wire: ab-initio simulations of fabrication driven fault tolerance

A. Pulimeno, M. Graziano, A. Sanginario, V. Cauda, D. Demarchi, G. Piccinini

***Abstract*—Molecular Quantum Dot Cellular Automata, also called mQCA, are among the most promising emerging technologies for the expected theoretical operating frequencies (THz), the high device densities and the non-cryogenic working temperature. Due to the small size of a mQCA cell, based on one or two molecules, the device prototyping and even a simple circuit fabrication are limited by the lack of control in the technological process. In this paper, we performed an analysis of the possible fabrication defects of a molecular QCA wire built with ad-hoc synthesized bis-ferrocene molecules. We evaluated the fault tolerance of a real QCA device and accessed its performance in non ideal conditions due to the fabrication criticalities we are facing in our experiments. We achieved these results by defining a new methodology for the fault analysis in the mQCA technology, based both on ab-initio simulations and theoretical computations. The results obtained give quantitative information on the Safe-Operating-Area (SOA) of a bisferrocene molecular wire, and represent an important feedback to improve the technological process for the final experimental set-up.**

***Index Terms*—Quantum Dot Cellular Automata, molecular QCA, ab initio simulations, molecular nanowire, defects modeling, safe operating area.**

I. Introduction

The reason at the root of the expectations on Quantum Dot Cellular Automata devices as succesfull CMOS substitutes [1] is that no charge transport is involved, but only local field interaction determines the information transfer. Power consumption is then expected to be dramatically reduced. Consequently, notwithstanding the increased device density, power densities would be more bearable than in the case of other nanoscale technologies based on electron transport, then improving expectations on reliability. Quantum Dot Cellular Automata (QDCA) [2][3], NanoMagnetic Logic (NML) [4][5][6] and Molecular Quantum Cellular Automata (MQCA) [7][8][9][10][11] are currently envisaged as the three possible implementations of the principle.

We focus on MQCA, which is considered the most promising for the expected operating frequencies. In particular we study a real molecule, a bis-ferrocene (Figure 1.A), specifically synthesized for this purpose [12][13] and that we are using for our own experiments. The technological process, though, both in general and specifically for this molecule, is currently lacking the proper control, and this explains the extremely reduced set of prototypes and experiments on this QCA type [14][15][16]. It is fundamental to be prepared to high defect rates and thus an assessment of the device fault tolerance is needed. On the other hand, a sound understanding of the device behavior in presence of defects helps giving the technologist crucial feedback on the directions to be followed when refining the process. These are the motivations guiding our work in the present contribution.

Azzurra Pulimeno, Mariagrazia Graziano, Danilo Demarchi and Gianluca Piccinini are with the Electronics and Telecommunication Department of Politecnico di Torino, Italy. Alessandro Sanginario, Valentina Cauda and Danilo Demarchi are with the Center for Space Human Robotics PoliTo, Istituto Italiano di Tecnologia, C.so Trento 21, 10129, Torino, Italy.

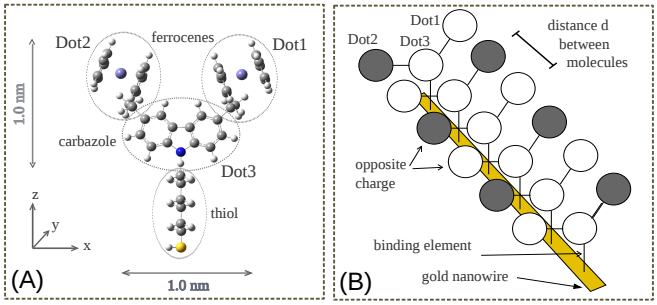

Fig. 1. (A) Bis-ferrocene molecule: two ferrocenes are linked together by means of a carbazole central group. These ferrocenes represent the two dots responsible for the logic state encoding, while the carbazole acts as the central third dot. An alkyl-chain provides the binding of the bis-ferrocene to the ending thiol (-SH) group. This end-group is responsible for the binding to the gold substrate, especially for the Self Assembled Monolayer formation. (B) Molecular QCA wire: bis-ferrocene molecules aligned over a gold nanowire.

From a methodology point of view, previous works related to QCA fault analysis referred to either available simulators like QCADesigner [17][18][19] or to models specifically developed for the purpose [20][21]. We aim at working as much as possible near the physical level in order to trim our experimental process and to understand the device behavior as much precisely as possible. We hence use *ab-initio* simulations and successive processing of the data we obtain, rendering the device behavior from an electronic point of view, more than from a chemical point of view.

In this study we refer to an experiment we aim at, thought for demonstrating the MQCA principle and the properties of bis-ferrocene. We focus on a *molecular QCA wire* (Figure 1.B) discussed in the following sections. As a consequence, when approaching the analysis of defects and of molecule fault tolerance, we refer to the physical properties of the materials involved in the case we are studying and experimenting on. We have thus a link to technology and give an unprecedented point of view on the subject. Moreover, the method is general and can be applied to other molecules and experimental setup related to MQCA.

We consider defects causing molecule displacement. We analyze a Molecule-Under-Test (MUT) misplaced with respect to a driver molecule and analyze the consequences on the

MUT ability to hold the information and to propagate it to a following molecule. Results are obtained for a large set of cases derived from the most probable defects that we expect from the technology we are considering.

To summarize, our main **contributions** in this paper are as follows:

- we identified the possible defects and causes of faults considering a real experiment on MQCA and a real molecule;
- we defined a new methodology to analyze the molecule behavior based on ab-initio simulations and on successive post-processing finalized to understand the electronic behavior of the molecule and of a molecular wire;
- we assessed the capability of the molecule to hold the information and to propagate it to a receiver as a function of the set of defects we identified; we can provide final Safe Operating Area (SOA) assessment and give feedback to the technologist to trim the next experimental steps.

The paper is organized as follows: in section II background is given on QCA and on the molecule we are focusing on; in section III we describe the type of defects we are considering in relation to our ongoing experimental procedures; in section IV we describe the methodology used to analyze the molecular wire and the set of simulations we executed; in section V we gather and comments the most relevant results, and conclude in section VI.

II. Background

A. QCA paradigm

In the early '90s, C.S. Lent and coworkers introduced the QCA theory as a new concept for digital computing [2], [3]. According to this new paradigm, a new device could be implemented by a cell with 6 dots containing two free charges. Depending on the positions of the free charges, three different states could be possible: when the two charges localize along one of the two diagonals, the logic 1 and logic 0 are encoded, as shown in Figure 2 (a); the configuration with the two charges in the central dots represents a NULL state, that is not a real logic state but it is necessary for the adiabatic switching [22], [8]. In particular, adiabatic switching consists of three consecutive steps: i) lowering the inter-dot potential barriers in order to remove the old state of the cell, ii) applying the new input to the cell and then iii) raising again the barriers in order to lock the cell in the new state. If these transitions are gradually applied, cells do not fall into a metastable state. This effect can be performed by applying an external electric field, called "clock signal". The interaction between two QCA devices is based on electrostatic repulsion; in this way simple logic gate could be implemented just placing QCA cells near each other in a specific layout. The free charges inside a cell will arrange in the configuration with the minimum energy, depending on the charge distribution of the previous cell, thus encoding a logic state and letting the information propagate. In this way, no current flow is required to perform a digital computation and this means a strong reduction of power consumption for QCA technology. The basic logic gates made of QCA cells are shown in Figure 2 (b), (c) and (d):

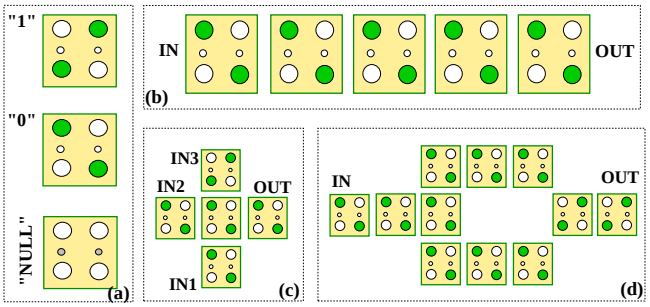

Fig. 2. QCA basic cell and basic blocks. (a) Six dots QCA cell: two free charges (filled circles) are localized along one of the two diagonals, encoding the 0 or 1 logic state; when the charges are forced by an external signal into the central dots the cell is in the NULL state. (b) A QCA wire: each cell along the line arranges its state according to its neighboring previous cell; when an external input forces a logic value on the extreme left cell (IN), then the binary information propagates along the wire to the extreme right cell (OUT) in a domino-like style. (c) A majority voter: the output depends on the state of the majority of the input cells. (d) A QCA inverter: output assumes the opposite value of the input.

a QCA wire, a Majority Voter and an Inverter, respectively. Using these gates as building blocks many complex digital systems could be designed, from arithmetic circuits [23] and also microprocessors [24].

Regarding the physical implementation, different possible solutions were proposed and discussed in literature and, among them, systems based on nano-magnet [4][5][6] and molecules are the most efficient and promising ones. A brief background on the latter follows.

B. Molecular QCA

According to the Lent theory [3], the smallest and most performing QCA cell could be implemented with a molecular system. Thanks to the nanometer size of many molecules, the operating temperature of molecular QCA circuits is not cryogenic and the device density of a chip increases leading to high complexity digital systems. In addition, theoretical frequencies up to THz are estimated.

In [7][8][25][14] some possible candidate molecules were presented: all these molecules are ideal systems and are studied in vacuum, so they are not suitable for a real circuit. Only one experimental attempts has been carried out on a mixed-valence complex [14][26], measuring a charge transfer in a film of molecules. However, a molecular QCA prototype has not been fabricated yet.

Recently, the authors in [12][13] synthesized a new molecule (bis-ferrocene) ad-hoc for QCA purpose: the structure of the molecule is reported in Figure 1 (A). The bis-ferrocene molecule is constituted by two bis-ferrocene units, where each ferrocene is linked to the next by a carbazole central group. The carbazole group shows an alkyl-chain to which an ending sulfur atom, actually a thiol (-SH), is attached. This end-group is responsible for the interaction with the gold substrate for the Self Assembled Monolayer (SAM) formation. The two ferrocenes represent the dot responsible for boolean encoding, while the carbazole acts as a central dot for the NULL state (and plays a role in case the clock signal is applied as we demonstrated in [11]). A molecule in

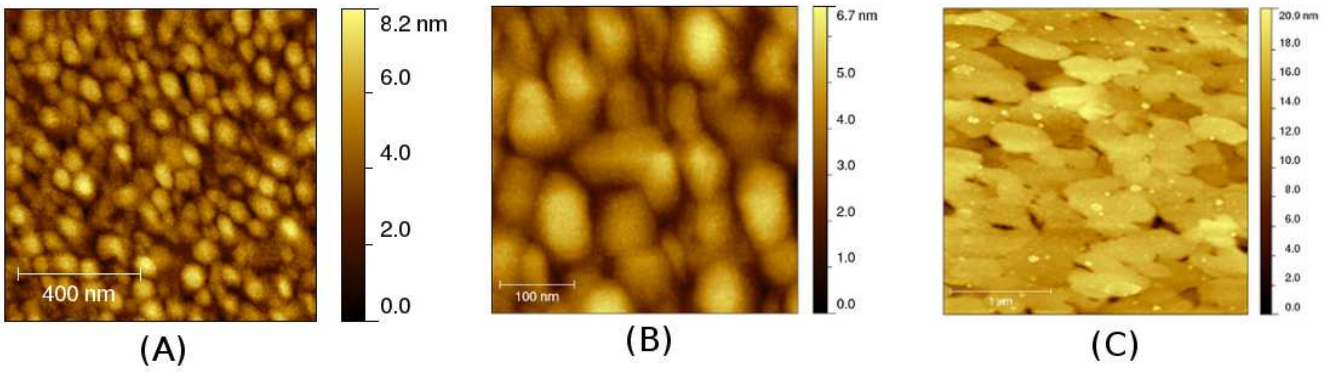

Fig. 3. (A) STM image of 1 μm^2 sputtered bare gold; (B) STM image of 500 nm^2: magnification of Figure 3.A; (C) STM image of 3 μm^2 epitaxial gold Au(111) thin film grown on mica substrate

both its oxidized and reduced states displays one or more free charges. In particular, in the case of the bis-ferrocene molecule, different oxidation processes were performed with good results [12][13]. Moreover, preliminary attempts of deposition on gold were already carried out for the formation of SAM with bis-ferrocenes [12][13]. In this work we focused on the oxidized form (a net positive charge inside the molecule) of the bis-ferrocene for our fault tolerance analysis in a molecular QCA wire.

Regarding the QCA cell and its functionality, since the molecule has only three dots, a complete QCA cell could be implemented placing two molecules near each other in such a way to obtain a square with the four boolean dots. The bistability of the the bis-ferrocene was already proved in [13][9] by means of ab-initio simulations. Moreover we analyzed the effect of a write-in system in [10] and simulated the presence of a "clock signal" in [11] to evauate the properties of the molecule in terms of QCA characteristics. Preliminary results showed promising behavior in presence of the clock field: a clear enhancement or reduction of molecule sensitivity to an input signal were revealed depending on the clock field value and direction.

III. Experimental related defect types

The literature shows remarkable contributions to the analysis of faults in QCA, confirming how carefully this issue is studied. In [27] the effects of cell radial displacement and missing dots defects on the operation of a QDCA wire are inspected. In [20] the behavior of QDCA devices in presence of cell rotation are analyzed and the allowable rotation angle is assessed through the definition of a new set of equations modeling the rotation effect. In [6] a NML logic block, the Majority Voter, is thoroughly simulated in presence of geometrical defects due to fabrication issues by means of detailed micromagnetic simulations.
For MQCA the authors in [21] analyze the behavior of building blocks in presence of random cell displacement, assessing tolerances, after the development of a model describing coherence vectors. In [19], a detailed characterization of defects and of their consequences on MQCA logic blocks are studied using QCADesigner simulations. In [18] authors refer to specific experimental data in [14][16] to model molecule deposition defects, like missing or additional MQCA cell. QCADesigner is used to investigate the effects of defects at device level and their consequences of logic blocks functional behavior.

In our case we refer to a specific experiment illustrating its preparation step by step. A description of the involved procedures is then presented: in some cases we have already results and measures to discuss about, in others we are running our experiments and still measurements cannot be shown. However, our knowledge of the procedure and of the problems arising during its execution allow us to identify the defects that could influence the final molecular wire organization. Consequently, a discussion on the related defects and of the faults classification follows the experimental description.

A. The experiment

We are preparing a bis-ferrocene molecular wire like the one in Figure 1.B, based on a gold nanowire upon which the molecules can be binded through the thiol element (Figure 1.A.) To achieve this experimental scheme, our idea is to prepare (phase I) a gold substrate as smooth as possible to avoid deposition defects and communication errors, and then (phase II) to reduce it to a single nanowire through optical and focus ion beam (FIB) lithography, nanopatterning and nanoimprinting [28][29][30]. Currently we are working on a wide gold area to assure the best properties of the substrate, whereas the future step will be the fabrication of a gold nanowire as a "guiding" element. We believe that the surface roughness should not increase after the realization of the nanowire. Moreover, we are working on the correct procedure to prepare the Self Assembled Monolayer that, in a first step (phase I) will cover the whole substrate (this is an ongoing work), and, in a second stage of the experiment (phase II), will be constrained on the nanowire only.

Substrate preparation. As we needed a gold surface as smooth as possible, the substrate also requires a very low roughness. To achieve a fairly good surface we smoothed a clean glass microscope slide following the procedure described in [31]. The surface roughness of glass (measured over the area of $1\mu m^2$) was Ra = 0.28 $\pm$ 0.05 nm (the average value from ten different measuring positions). Then we sputtered 100 nm

of gold using a low deposition rate (0.05 nm/s) to achieve a good homogeneity of the film as demonstrated by [33].

Figures 3.A and 3.B show a Scanning Tunneling Microscope (STM) image of the gold layer obtained from the process described above. If we exclude outliers, the surface presents grains with an average diameter of 80 nm $\pm$ 5 nm and an average displacement along the z-axis of 2 nm $\pm$ 0.5. The mean roughness of each grain is 0.20 nm $\pm$ 0.1 nm. As can be clearly noticed, the grains conformation is eggs-like. The height between the base and the top of the hills is about 2 nm $\pm$ 1 nm. The distance between grains ranges between 2 nm and 6 nm. As a consequence, in this work we executed ab-intio simulations considering a *displacement of the molecules* along the three axes (see later in subsection B).

A possible solution to avoid this problem is to use a flatter gold surface like the 150 nm Au(111) thin film on mica substrates (from Jeol). Gold on mica substrates present very flat and oblong terraces (see figure 3.C) with average dimensions of about 300x600 nm. Moreover the roughness of these terraces is 0.1 nm $\pm$ 0.05 nm.

Molecule deposition. This part of the experiment is still on-going and measurements are preliminary. However, we illustrate them here so that a useful classification on possible defects can be presented afterwards. A Self Assembled Monolayer (SAM) of bis-ferrocene molecules [12][13] was prepared in two steps. First, the gold (111) substrates were incubated into a solution 1 mM of hexane-1,6-dithiol in absolute ethanol (EtOH) at room temperature. The substrates were then gently rinsed with EtOH and dried under nitrogen flow. For the second step, the Au (111) substrate with the first SAM were again incubated into a solution of 1 mM of bis-ferrocene molecule in EtOH, then gently washed in clean EtOH and dried under nitrogen. The as-prepared SAM was then used for AFM investigation and experiments are currently on-going. Control experiments were carried out with clean Au(111) on mica substrates and SAM of only hexane-1,6-dithiol on Au(111).

A first origin of *fault* in the preparation of a molecular wire for QCA operation is attributed to the huge steric hindrance of the bis-ferrocene molecule used here. In this geometrical configuration, the solid-state immobilization of the bis-ferrocene molecule implies the anchoring of the disulfide group (S-S) to the gold surface. Thus in the SAM, the two ferrocene units might be unable to be vertically oriented with respect to the substrate, and slightly tilted away from the vertical position, due to the steric hindrance of the huge bis-ferrocene groups. However, this geometrical configuration should not prevent at all the Boolean state operation in the single bis-ferrocene molecule. Similarly, the steric hindrance of the ferrocene units can prevent the close vicinity of other molecules and thus QCA operation. If two cells are too far away from each other, with an *inter-distance* exceeding their interaction through the electrostatic field, no Boolean operation might occur among them.

Another possible problem in the formation of a molecular wire for QCA operation relies on the bis-ferrocene *intercalation* into the already formed hexane-dithiol SAM, during the incubation of the hexane-dithiol SAM on the Au(111) substrate with the bis-ferrocene solution (second step of the molecule deposition process). It is possible indeed that the very good packaging of the hexane-dithiol molecules prevents the insertion of the bulky bis-ferrocene ones. This could result in the absence of intercalation and a huge distance between one bis-ferrocene unit to the next one, preventing the formation of a continuous molecular wire and further QCA operations.

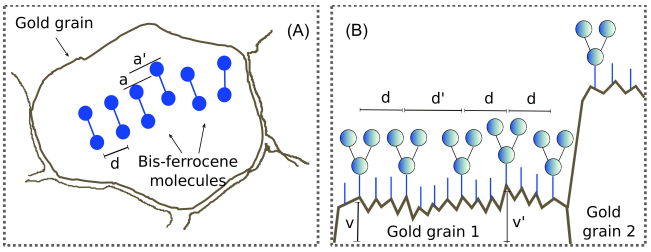

Fig. 4. Fabrication defects in the case of a QCA wire made of bis-ferrocene molecules. (a) Top view of a gold grain after molecule deposition: misalignment and tilt defect are sketched. (b) Section of a bis-ferrocene SAM on gold: vertical shifts may occur due to the roughness inside a gold grain or at the interface of two grains. In addition, a different number of spacers (thiols) between two molecules may lead to a variation of the distance d.

A final consideration should be done on the source of defects due to the *synthesis* of the molecule. A missing ferrocene or an additional ferrocene, or an incorrect molecule organization might be possible. However, this is considered a rare event, compared to the previously mentioned defects cases [18][12].

B. Classification

A schematic view of the possible defects related to the experimental setup we are working on is in Figure 4. A top view of the gold grain structure is in Figure 4.A, where a wire of molecules is displayed. In this picture, for the sake of a simple and clean classification, the molecules are supposed to form a single wire, even though the substrate is not yet a nanowire. In case molecules are not constrained on top of a nanowire, indeed, more likely also other "parallel" competitive molecules could be present. However, the case is not considered as we suppose to work on the "guiding" gold nanowire as a final step. A **reference distance** d is expected between two consecutive molecules. A **reference alignment** a, proper of a SAM, is expected in terms of dot position, as mentioned in the preparation procedure. However, during the experimental processes discussed in section III-A some errors might occur and they are schematically depicted in Figure 4. In particular: i) the steric hindrance could lead to a molecule rotation; ii) a misalignment of dots (see Fig. 4.A) is due to an incorrect binding caused by the defects of the gold grain or by the irregularity of the hexane-ditiol SAM. Moreover, iii) the presence of hexane-ditiol elements between consecutive molecules with the incorrect concentration could increase or decrease the distance d, as shown in Figure 4.B. Molecules, iv), might be placed on different grains, thus causing a huge vertical distance between dots. However, v) also molecules bound on the same grain might experience the grains roughness and dots could be vertically displaced,

instead of assuming a **reference vertical position** v (see Fig. 4.B).

We can at this point classify the REAL possible defects we should consider herein. A view of Figure 6 (discussed in the next section) might also help the visualization of the following statement.

X displacement: considering an expected *reference alignment* a in which the dots of two molecules are perfectly faced ($a = 0nm$), a displacement might occur along the X axis, both in the positive and negative direction, and defined as $delta\,X$.

Y displacement: considering an expected *reference distance* d which corresponds to the distance between the two dots ($d = 1nm$), a displacement might occur along the Y axis (refer to Figure 1.A axes reference), both positive or negative, defined as $delta\,Y$.

Z displacement: considering an expected *reference vertical position* v, a vertical displacement might occur along the Z axis, both as positive or negative $delta\,Z$.

Orientation variation: a mix of X and Y displacements might occur.

Missing molecule: an extreme case of both X and Y and Z displacements might occur.

Missing dot: due to defects at the synthesis stage, molecules might present only one dot.

Additional dot: due to synthesis stage as well.

As explained in the following section, we decided to focus on the most important ones, the X, Y and Z displacement considered singularly. The gold standard used as reference point corresponds to a reference X,Y and Z considered as ideal conditions.

The defects we mentioned might cause cell **faults** that are studied in this work and discussed in the results section. Faults expected are: i) cell mis-behavior in holding the information, ii) cell mis-behavior in propagating the information, iii) cell inability to switch in presence of external signal (stuck-at), iv) cell impossibility to receive the information.

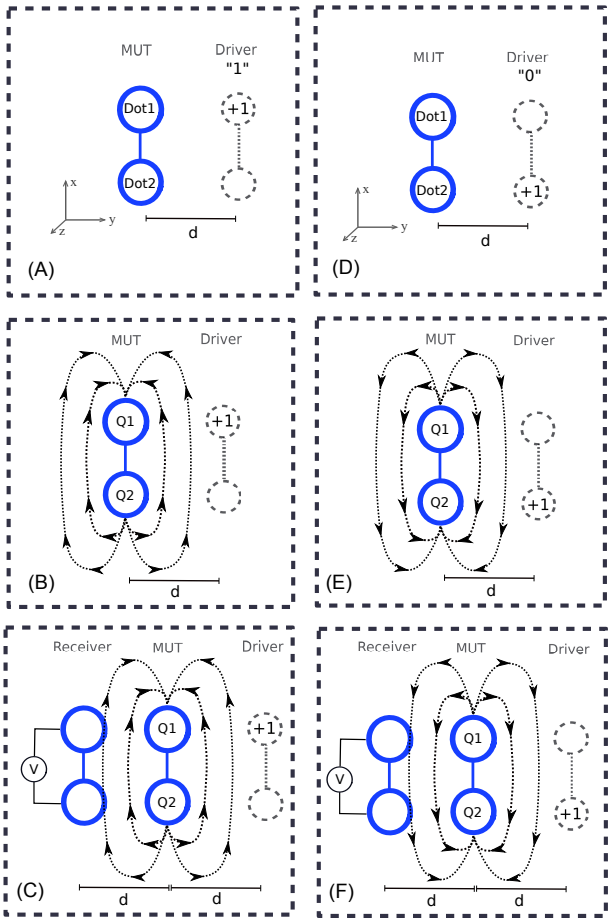

Fig. 5. The analysis flow we adopted is divided into three steps: (A), (D) firstly, we emulated the presence of an ideal driver placed at a distance d equal to the width of the molecule under test (MUT), in order to obtain a square with the four dots. The driver should represents a molecule with a free charge localized in on of the two dots; therefor, a point charge equal to +1q is aligned with the dot1 (and then dot2) of the MUT, emulating a logic state 1 (logic state 0). (B), (E) The presence of the driver influences the logic state of the MUT, so that the dot charges (*Q1* and *Q2*) vary. (C), (F) We estimated the effects of the electric field generated by the charge distribution of the MUT and we computed the equivalent voltage measured at an ideal receiver placed at the same distance d from the molecule.

IV. Methodology

In order to evaluate the fault tolerance of a molecular QCA wire, we defined a methodology flow as shown in Figure 5. Our analysis focuses on a system composed of an ideal emulated *driver*, a bis-ferrocene *molecule under test* (MUT) and an ideal *receiver*, as part of the molecular wire. The aim is to evaluate the bistability of the MUT and its capability to propagate the information in presence of fabrication defects. In particular, since we consider the bis-ferrocene in its oxidized form (a net positive charge), we emulated the ideal driver as a point charge equal to *+1 q*, that means a molecule with a localized positive charge. The driver is placed at a distance d equal to the distance between dot1 and dot2, so that a 4 dots square is formed. Moreover, the localization of the point charge determines the logic state of the driver: when the charge is aligned with the dot1 of the MUT, the driver is in the logic state 1 (Figure 5.A). Otherwise, the alignment to dot2 encodes the logic state 0 (Figure 5.D). In this way, we force a value at the input of the QCA wire and expect a consequent arrangement of charge inside the MUT, depending on the driver logic state (Figure 5.B and E). The dot charges of the MUT (*Q1* and *Q2*) determine the state of the MUT itself; the charge difference between the dots generates an electric field. Then, we emulated an ideal receiver that acts as the third molecule of a wire (Figure 5.C and D): the electric field generated by the MUT is responsible of the state switching at the receiver, and so of the information propagation.

Referring to the classification assessed in section III, we modeled three types of defects varying the position of the driver. In Figure 6 a sketch of this model is reported: firstly, we considered the misalignment of the driver with respect to the two dots ($delta\,X$, Figure 6.A), due to defects in the orientation of the gold grain (see Figure 4.A). Then, we varied the distance between the driver and the MUT ($delta\,Y$) to model a non ideal square cell (Figure 6.B) in case of different number of spacers between two molecules as depicted in Figure 4.B. Finally, the roughness of gold grain is modeled as the shift of the driver along the vertical axes of the MUT

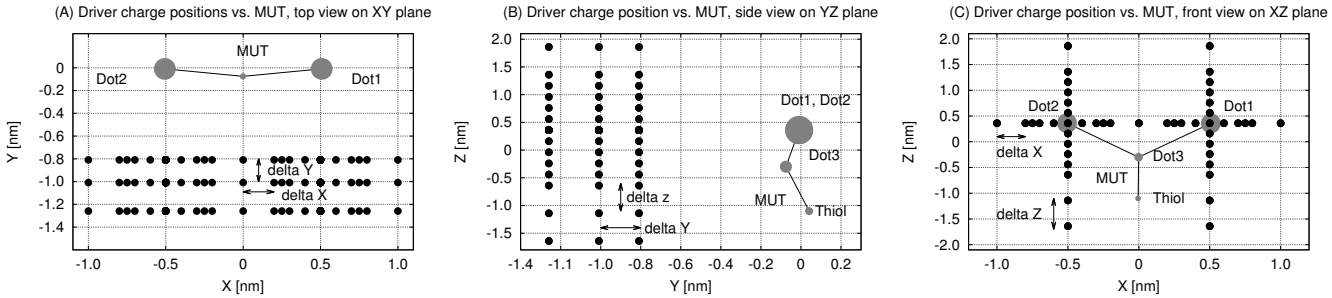

Fig. 7. Simulation points: (a) top view, (b) section view and (c) lateral view. Each filled circle represents the position of the driver and its displacement from the molecule in our fault analysis scheme.

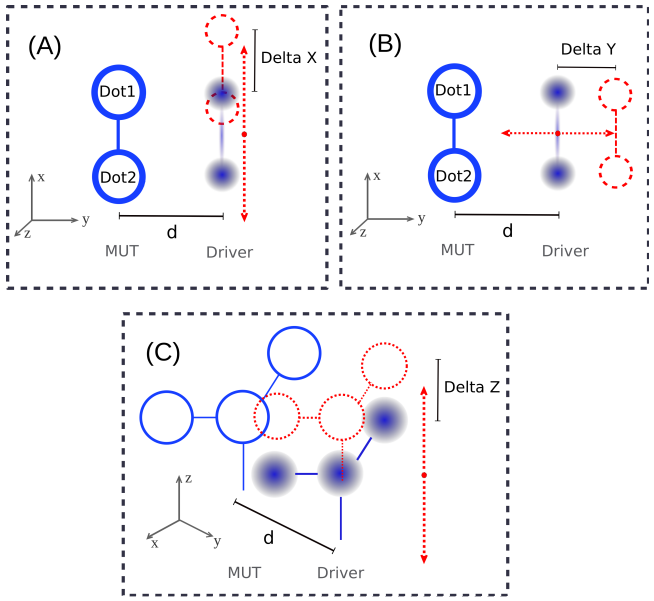

Fig. 6. Fault types analysis: we emulated three possible fabrication defects, moving the driver with the respect to its ideal position. In particular, we evaluated the bistability of the molecule when the driver is not perfectly aligned with the two dots (A), when it is placed at a distance different from the ideal d (B), and when the displacement is along the vertical axes of the molecule (C). In all the Figures, black circles represent the position of the point charge.

shown in Figure 6.C ($delta\ Z$).

Our methodology is based on ab-initio simulations performed with Gaussian09 [32] at room temperature. For a complete overview of our fault type analysis, in Figure 7 all the simulation points are reported: each black circle represents a spatial position of the point charge with the respect to the MUT. In this figure all the variations from the ideal position along the three axis can be appreciated.

Since the charge localization inside the molecule is the main requirement for QCA bistability validation, we need to evaluate the charge distribution of the MUT under different bias conditions (different positions of the driver). So, we calculated the atomic charge of the molecule and we then defined the **aggregated charge** as a simple sum of the atomic charge of each atom that forms a specific site of the molecule (in this case dot1, dot2, dot3 and thiol, see also Figure 1.A). In our methodology scheme (Figure 5), *Q1* and *Q2* are the aggregated charges for dot1 and dot2, respectively. Hereinafter we refer to dot1, dot2, dot3 and thiol charges as the aggregated charges of these parts of the bis-ferrocene molecule.

As a figure of merit at the receiver level, we computed the **electric field** generated by a charge system. In particular, the charge distribution of the MUT under different biases is the input system and the electric field is computed at a distance d from the molecule. In this way an ideal receiver is emulated to form a 4 dots square QCA cell with the MUT. In order to evaluate the possibility to propagate the information when a defect occurs, we defined an **equivalent voltage at the receiver**, that is a figure of merit analytically derived from the generated electric field. Finally, to assess the fault tolerance of a molecular QCA wire in case of different fabrication defects, we defined a **Safe Operating Area (SOA)** in which we highlighted the working points of the receiver in case of spatial displacement. In particular, to determine whether a point is still suitable for the correct computation, we checked if the receiver was able to switch following the MUT changing of state. In order to validate this points, we used the equivalent voltage at the receiver and defined three different threshold voltages. Defined an area of interest equal to a 4nm x 4nm square centered on the MUT, the SOA is evaluated separately for different driver positions. The electric field generated by the MUT for the two logic states of the drivers are used to define the SOA: the receiver is moved rastering the area of interest. For each point the equivalent voltage at the receiver is evaluated for both logic state 0 and 1 of the driver. These equivalent voltages were defined as V_{rx0} and V_{rx1}, respectively. We identified a set of threshold voltages (V_{th}), ranging from 0.1 to 0.9 V. The point (x, y) is considered safe for any V_{th} if the following condition is satisfied: $V_{rx1}(x, y) > |V_{th}|$ and $V_{rx0}(x, y) < |V_{th}|$.

V. Results

In Figure 8 the electric fields generated by a molecule under the influence of a driver are shown. In the left figure, the curves are computed using all the atomic charges as input system; whereas the results in the right figure are obtained with the aggregated charge [10]. This is one example of the extensive analyses we performed to define in what extent the aggregated charge can be used to model the molecule behavior from an application point of view. Since the trend of the electric field computed with the aggregated charges is practically the

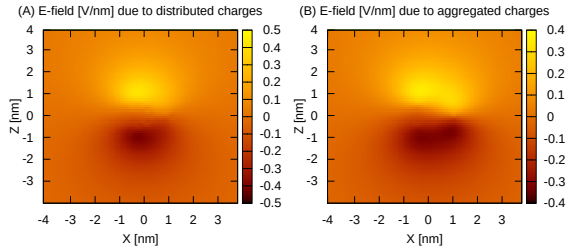

Fig. 8. Electric field generated by the MUT in standard position when subject to an active driver. Field is computed both using the charges of all the molecule atoms (left) and the aggregated charge approximation (right) and measured in the XZ plane at a fixed distance from the molecule, equals to 1.0 nm along the Y direction. It could represent the electric field a nearby molecule, called receiver, is subjected to.

same of the case with all the atomic charges, we could assess that performing our analysis using the new figure of merit, defined as aggregated charge, does not affect the accuracy of our results.

On the basis of this consideration, we computed the dot charges of the MUT in different bias conditions (corresponding to different positions of the driver) in order to simulate the possible fabrication defects. Figure 9 reports the results for the driver shifting along the vertical axes, that we called *delta Z*: the top figure is related to driver logic state 0, while the bottom one to driver logic state 1. Both graphs include the results for three different distances from the MUT (equivalent to three values of *delta Y*). For the two logic states, the charge difference between the two dots decreases when the value of *delta Z* is incremented. This is enhanced for longer distances from the molecule (higher *delta Y*). In particular, in the range related to the roughness of the gold substrate inside a grain ($\pm 0.2 \div 0.4nm$) the molecule still works properly, that means that the free positive charge is mainly localized on one of the two dots, encoding a valid logic state. On the contrary, when the driver-MUT interaction is at the interface between two gold grains (equivalent to *delta* $Z = \pm 2.0nm$) the molecule is in an undefined state, because the charge of the two dots is almost the same. Referring to the faults classification defined in section III, as far as vertical displacement is concerned the cell is unable to receive the information if the driver is on another gold grain. On the contrary, at least for the MUT alone, a molecular wire all constrained in the same grain assure a proper behavior. The technologist can be satisfied with the process adopted for assuring the correct roughness. However, thinking at both the final experiment and future more complex circuits, grains should be as big as possible.

Regarding the driver misalignment with the respect to the two dots (*delta X*), the trend of the dot charges is reported in Figure 10. Also in this case, three different distances (*delta Y*) are considered, so the left graph refers to the smallest distance, the central to the ideal one and the third graph is related to the highest distance. In all these graphs, the curves for both the cases of driver logic state at 1 and at 0 are reported simultaneously, in order to check immediately the MUT bistability for a specific driver position. In particular,

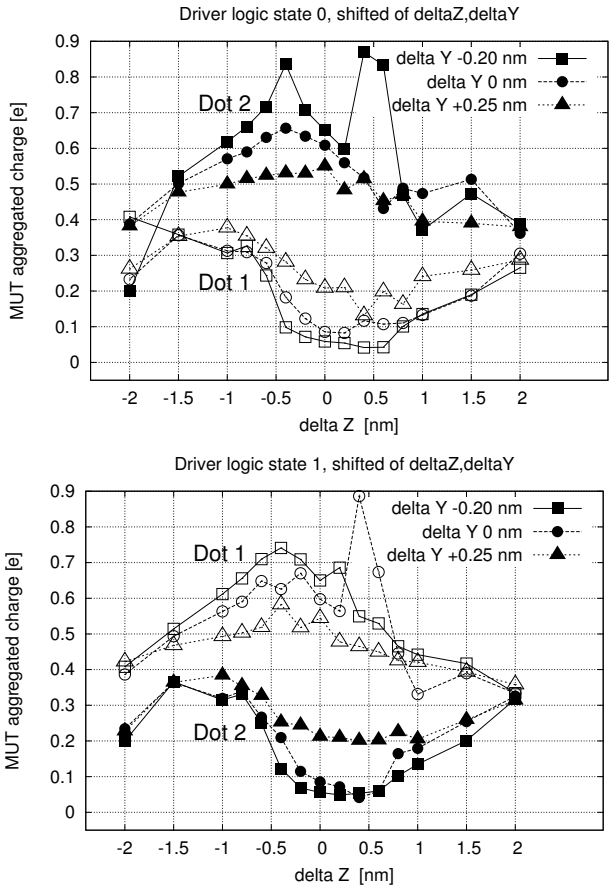

Fig. 9. Dot charges as function of the driver shifting along the vertical axes (*delta Z*) for three different distances from the molecule (*delta Y*). In the top figure the driver is set to a logic 1, while in the bottom one the driver state is logic 0. For both the cases, filled points are for dot1 and empty points for dot2.

for a given *delta X* value it is possible to check if the dot charges switch moving from driver at 1 to driver at 0 and the difference between them is great enough to be considered a valid state. This means that the MUT could work properly. On the contrary, in case of no switch or no difference between the two dot charges, a stuck-at occurs or the MUT is in an undefined state. The results shown in Figure 10 reveal that there is a wide range of fault tolerance for the smallest and the ideal distance, while for the greatest one this range is notably reduced.

Our methodology flow ends with an analysis of the MUT capability to propagate the information in presence of a driver defect. This step is performed computing the electric field generated by the charge distribution of the MUT in all the above mentioned cases of driver displacement. In particular, the intensity of the electric field is measured emulating an ideal receiver (a sort of electric field sensor, that should act as the third molecule of a wire) placed at the reference distance *d* from the molecule. From the electric field values obtained and considering the width of the molecule (1 nm, see Fig. 1.A), we calculate the equivalent voltage at the receiver. The results of this analysis are shown in Figure 11: these graphs are strictly related to the curves in Figure 10, since they are computed on

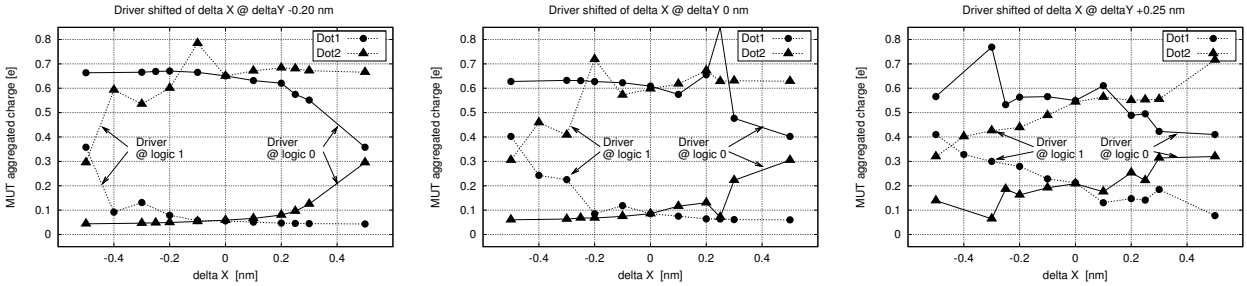

Fig. 10. Dot charges as function of the driver misalignment with the respect of the two dots (delta X). Left, central and right figure are related to three different distances from the molecule (delta Y). In all the cases, dashed lines refer to logic state 1 of the driver, while filled lines are for logic state 0.

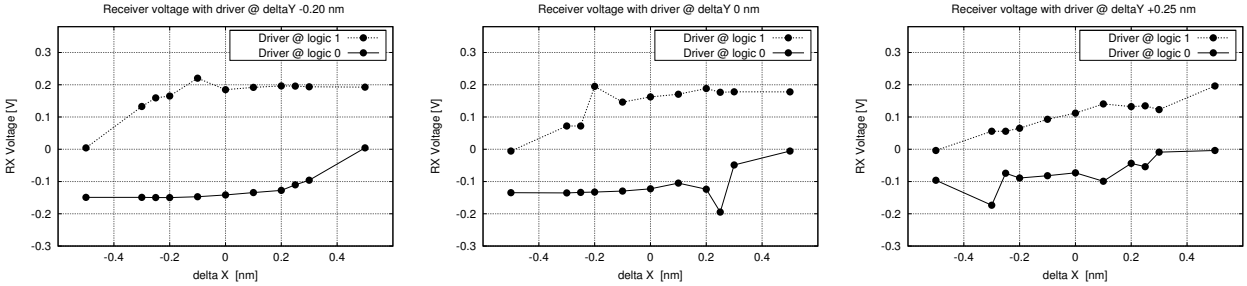

Fig. 11. Equivalent voltages at the receiver as a function of the misalignment of the driver (delta X). Left, central and right figure are related to three different distances from the molecule (delta Y). In all the cases, dashed lines refer to logic state 1 of the driver, while filled lines are for logic state 0.

the basis of those charge data. The driver defects that allow a correct information propagation are the ones in which the voltage reveals a change of sign when the driver changes its state (switching). In addition, the absolute value of the voltage should be the value required to switch the receiver state. As shown in Figure 11, small perturbations from the ideal position do not affect the communication in all the three cases of *delta Y*; however, higher values of *delta X* could be acceptable only for smaller *delta Y*.

Finally, to enrich our fault tolerance analysis, we emulated also the simultaneous concurrency of driver and receiver defects: we moved the receiver on the whole XY plane (no vertical shifting) and measured the voltage for some corner cases in terms of driver defects. Following the methodology described in section IV, we drew a Safe Operating Area (SOA) in which the working points are outlined. In particular, these points correspond to the center of the receiver molecule. Figure 12 shows the results for a set of driver positions, that are relevant to identify the possible fabrication defects. Each row corresponds to a different case of relation between the driver and the receiver: figure on the left (e.g. A1) represents the SOA, while the scheme on the right (e.g. A2) gives an idea on molecules displacement.

Figure 12(A) is related to the ideal position of the driver: the points in the XY plane, in which the receiver (the center between the receiver's two dots) could be placed to assure a correct propagation of the two logic states, are reported. The two circles represent the position of the MUT, which is fixed. As shown in this figure there are different regions in which the equivalent voltage at the receiver varies from 0.1 V to 1.0 V. Moreover, the receiver tolerates better a variation of the distance from the molecule (*Delta Y*) than a misalignment of the dots (*Delta X*), since the safe points extend more along the Y direction.

Considering a defect of the driver in the alignment with the respect of the molecule (*Delta X = 0.5 nm*, Figure 12(B)), the region where the receiver could be safely placed is a little bit wider than the previous case, especially in the Y direction, but the equivalent voltage at the receiver is quite lower.

A vertical shifting of the driver due to the roughness of the substrate (*Delta Z = 0.2 nm*, Figure 12(C)), is reflected at the receiver level with a SOA that includes a wide range of both misalignments and higher distances from the molecule. Moreover, the values of the equivalent voltage at the receiver are intermediate, confirming again that the gold roughness (0.20 nm $\pm$ 0.1 nm) obtained at the experimental level does not affect the information propagation.

In case of a bigger vertical shifting of the driver (*Delta Z = 0.8 nm*, Figure 12(D)), the charge distribution of the molecule is such that the SOA for the receiver is quite limited. Combining a vertical shift and a variation in the driver-molecule distance (*Delta Z = 0.4 nm* and *Delta Y = -0.2 nm*, Figure 12(E)), the effects at the receiver level are quantified in a very small SOA, mainly localized near the molecule, with low values of equivalent voltage.

Therefore, this analysis reveals that the tolerance of the QCA wire to some possible defects in the fabrication of the QCA wire is quite good. In addition, the results obtained and the data highlighted in 12 give an important feedback to the technologist about which are the critical points and which could be the improvement to assure a correct information propagation.

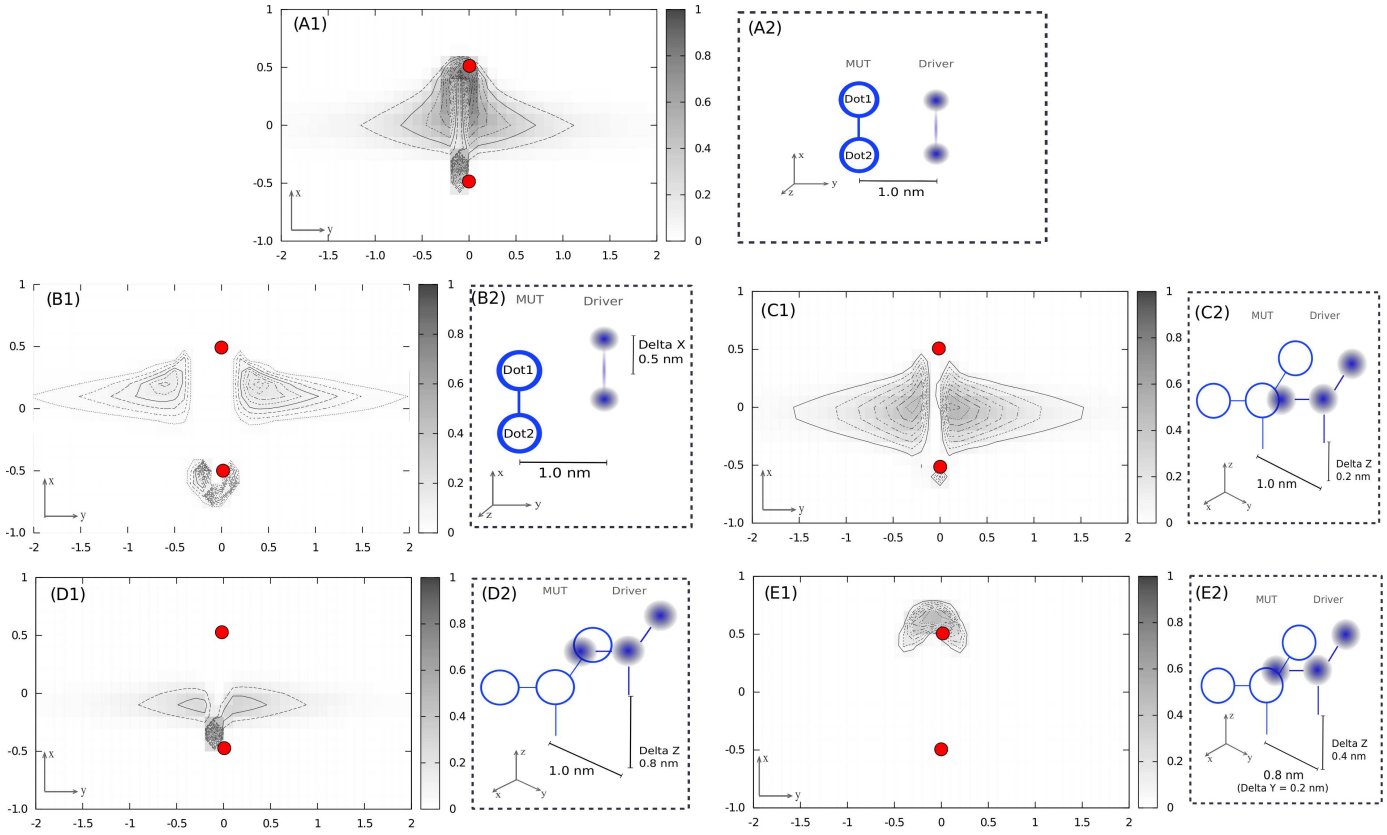

Fig. 12. Safe operating area (SOA) for corner cases in terms of driver defects. The gray points represent a working point on the XY plane where the receiver could be placed (center between the two dots of the receiver). Each SOA considers the MUT charges for both state 1 and 0 of the driver and highlights where the bistability of the receiver is satisfied. The MUT position is highlighted in all the graphs with the two circles. Figures named with different letters represent cases of SOA due to different displacement of the driver (e.g. A1, B1 etc...), specified in the right picture in each case (e.g. A2, B2 etc...).

VI. Conclusions

The results we obtained through ab-initio simulations on a real MQCA molecule are fundamental to address the fabrication of a molecular QCA wire on gold. In particular, the fault tolerance analysis discussed in this work highlights the feasibility and functionality of the MQCA wire also in presence of several defects we faced during our experimental processes: roughness of the gold substrate, misalignment of deposited molecules, variations of the distance of two nearby molecules. Considering these fabrication criticalities we evaluated the MQCA cell performance and the information propagation along the wire. Thanks to our methodological approach we could draw the Safe-Operating-Area (SOA) of a bis-ferrocene molecular wire. These results are promising for the development of molecular QCA circuits and, in the same time, give an important feedback to improve the technological process.

References

[1] Semiconductor Industry Association, “International Technology Roadmap of Semiconductors, 2010 Update, Emerging research Device (ERD)”. [Online]. Available: http://public.itrs.net, 2010.

[2] C.S. Lent, P.D. Tougaw and W. Porod, ”Quantum cellular automata: the physics of computing with arrays of quantum dot molecules”, IEEE PhysComp?94, pp.5-13, 17-20, Nov 1994

[3] C.S. Lent, P.D. Tougaw,W. Porod, and G. Bernstein, ”Quantum cellular automata”, Nanotechnology, vol. 4, pp. 49-57, 1994

[4] A. Imre, G. Csabaa, G.H. Bernstein, W. Porod and V. Metlushkob, ”Investigation of shape-dependent switching of coupled nanomagnets”, Superlattices and Microstructures, vol. 34, pp. 513-518, 2003.

[5] M. Graziano, M. Vacca, A. Chiolerio, M. Zamboni, “A NCL-HDL Snake-Clock Based Magnetic QCA Architecture”, IEEE Transaction on Nanotechnology, vol. 10 n. 5, pp. 1141-1149.

[6] M. Vacca, M. Graziano, M. Zamboni, “Majority Voter Full Characterization for NanoMagnet Logic Circuits”, IEEE Transaction on nanotechnology, Vol. 11, N. 5, pp.940-947, 2012.

[7] C. S. Lent, B. Isaksen and M. Lieberman, ”Molecular Quantum-Dot Cellular Automata”, J. Am. Chem. Soc., vol. 125, pp. 1056-1063, 2003

[8] C.S. Lent and B. Isaksen, ”Clocked molecular quantum-dot cellular automata”, Electron Devices, IEEE Transactions on, vol.50, no.9, pp. 1890-1896, Sept. 2003

[9] A. Pulimeno, M. Graziano, C. Abrardi, D. Demarchi, and G. Piccinini, ”Molecular QCA: A write-in system based on electric fields”, IEEE Nanoelectronics Conference (INEC), vol., no., pp.1-2, June 2011

[10] A. Pulimeno, M. Graziano, D. Demarchi, and G. Piccinini, ”Towards a molecular QCA wire: simulation of write-in and read-out systems” Solid State Electronics, Elsevier, vol. 77, pp. 101-107, 2012.

[11] A. Pulimeno, M. Graziano, and G. Piccinini, ”Molecule Interaction for QCA Computation”, IEEE NANO2012 12th International Conference on Nanotechnology, Birmingham (UK), 20-23 August 2012.

[12] L. Zoli, PhD Dissertation, Universitaḑi Bologna, 2010.

[13] V. Arima, M. Iurlo, L. Zoli, S. Kumar, M. Piacenza, F. Della Sala, F. Matino, G. Maruccio, R. Rinaldi, F. Paolucci, M. Marcaccio, P.G. Cozzi and A.P. Bramanti, ”Toward quantum-dot cellular automata units: thiolated-carbazole linked bisferrocenes”, Nanoscale, vol. 4, pp. 813-823, 2012

[14] Z. Li, A. M. Beatty and T. P. Fehlner, ”Molecular QCA Cells. 1. Structure and Functionalization of an Unsymmetrical Dinuclear Mixed-Valence Complex for Surface Binding”, Inorg. Chem., vol. 42, pp. 5707-5714, 2003

[15] H. Qi, S. Sharma, Z. Li, G. L. Snider, A. O. Orlov, C. S. Lent and T.P. Fehlner, "Molecular Quantum Cellular Automata Cells. Electric Field Driven Switching of a Silicon Surface Bound Array of Vertically Oriented Two-Dot Molecular Quantum Cellular Automata", J. Am. Chem. Soc., vol. 125, pp. 15250-15259, 2003

[16] J. Jiao, G.J. Long, F. Grandjean, A.M. Beatty and T.P. Fehlner, "Building Blocks for the Molecular Expression of Quantum Cellular Automata. Isolation and Characterization of a Covalently Bonded Square Array of Two Ferrocenium and Two Ferrocene Complexes", Journal of Americal Chemical Society, Communications, 125, 2003.

[17] http://www.mina.ubc.ca/qcadesigner_manual

[18] M. Momenzadeh, M. Ottavi and F. Lombardi, "Modeling QCA Defects at Molecular-level in Combinational Circuits", Proc. of 20th IEEE international Symposium on Defect and Fault Tolerance in VLSI Systems (DFT'05)

[19] M.B. Tahoori, J. Huang, M. Momenzadeh and F. Lombardi, "Testing of Quantum Cellular Automata", IEEE Transaction on nanotechnology, Vol3., N.4, December 2004.

[20] X. Yang, L. Cai, S. Wang, Z. Wang and C. Feng, "Reliability and Performance Evaluation of QCA Devices With Rotation Cell Defect", IEEE Transaction on nanotechnology, Vol. 11 N.5, 2012.

[21] G. Schulhof, K. Walus and G.A. Jullien, "Simulation of Random Cell Displacements in QCA", ACM Journal on emerging Technologie in Computing Systems, Vol.3, N.1, 2007.

[22] C.S. Lent and P.D. Tougaw, "A Device Architecture for Computing with Quantum Dots", Proceedings of the IEEE 85, pp. 541-557, 1997.

[23] G. Csaba and W. Porod, "Simulation of field coupled computing architectures based on magnetic dot arrays", *Journal of Computational Electronics,* Kluwer, V. 1, , pp. 87-91 (2002)

[24] K. Walus, M. Mazur, G. Schulhof, G. A. Jullien, "Simple 4-Bit Processor Based On Quantum-Dot Cellular Automata (QCA)", *I*ntl. Conf. on Application-Specific Systems, Architecture and Processors, ASAP, pp. 288 - 293, Nov. 2005

[25] Y. Lu, C.S. Lent, "Theoretical Study of Molecular Quantum-dot Cellular Automata," Journal of Computational Electronics, Vol. 4, pp. 115-118, 2005

[26] R.A. Joyce, H. Qi, T.P. Fehlner, C.S. Lent, A.O. Orlov, G.L. Snider, "A system to demonstrate the bistability in molecules for application in a molecular QCA cell", IEEE Nanotechnology Materials and Devices Conference, pp. 46-49, 2-5 June 2009

[27] M. Khatun, T. Barklay, I. Sturzu, P.D. Turgaw "Fault tolerance properties in quantum dot cellular automata devices", L.Phisics D.:Applied Physics, Vol. 39, N.8, pp 1489-1493, 2006.

[28] O. Fenwick, L. Bozec, D. Credgington, A. Hammiche, G.M. Lazzerini, Y.R. Silberberg and F. Cacialli, "Thermochemical nanopatterning of organic semiconductors". Nature Nanotechnology, 4 (10), 2009, pp. 664-668.

[29] P. Motto, A. Dimonte, I. Rattalino, D. Demarchi, G. Piccinini, and P. Civera, Nanogap structures for molecular nanoelectronics., Nanoscale Res Lett, vol. 7, no. 1.

[30] S. Strobel, S. Harrer, G. Penso Blanco, G. Scarpa, G. Abstreiter, P. Lugli, and M. Tornow, "Planar Nanogap Electrodes by Direct Nanotransfer Printing", Small, vol. 5, 2009.

[31] L. D. Eske and D. W. Galipeau "Characterization of SiO2 surface treatments using AFM, contact angles and a novel dewpoint technique", Colloids and surface A: Physicochemical and Engineering Aspects ,1999, vol. 154, pp 33-51

[32] M. J. Frisch et al. "Gaussian 09 Revision A.1", Gaussian Inc. Wallingford CT 2009.

[33] V. vork, J. Siegel, P. utta, J. Mistrk, P. Janek, P. Worsch and Z. Kolsk "Annealing of gold nanostructures sputtered on glass substrate", Applied Physics A: Materials Science & Processing, 2011, vol. 102, No. 3, pp 605-610